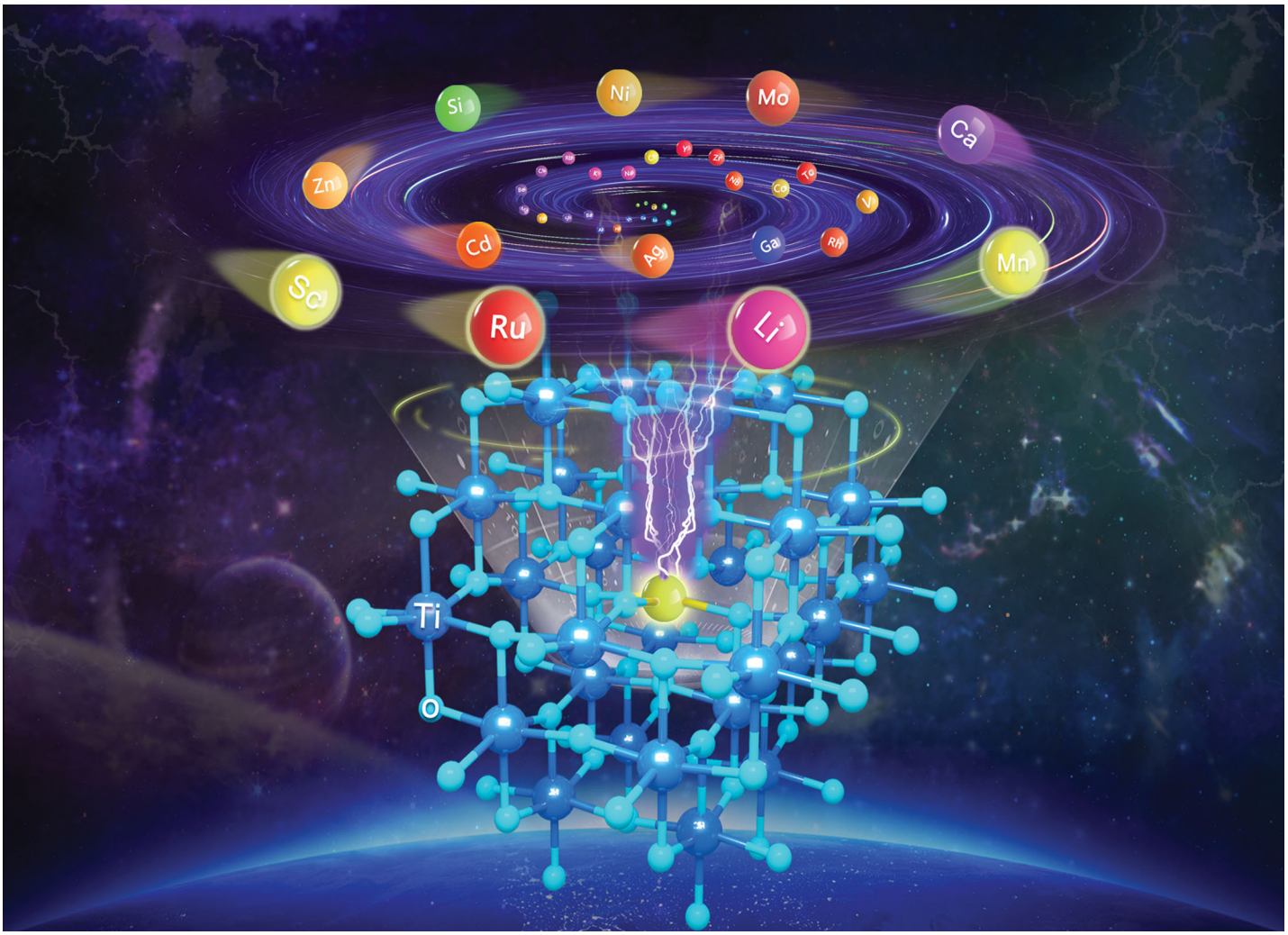

Showcasing research from the group of Prof. Feng Pan, School of Advanced Materials, Peking University Shenzhen Graduate School, China

High-throughput HSE study on the doping effect in anatase TiO_2

This work systematically studied the doping effects of 40 kinds of elements in anatase TiO_2 by high-throughput HSE06 calculations. It is found that doping with most of these elements can narrow down the band gap of TiO_2, while the recombination center induced by intermediate bands is also observed in some doped systems. Based on a more accurate method of calculation and uniform parameters, our work provides meaningful guidelines on designing photocatalytic devices based on doped anatase TiO_2 with high performance.

As featured in:

See Jiaxin Zheng, Feng Pan *et al.*, *Phys. Chem. Chem. Phys.*, 2020, **22**, 39.

ROYAL SOCIETY OF CHEMISTRY

rsc.li/pccp

Registered charity number: 207890

PCCP

PAPER

View Article Online
View Journal | View Issue

Cite this: *Phys. Chem. Chem. Phys.*, 2020, **22**, 39

High-throughput HSE study on the doping effect in anatase TiO_2†

Jiahua Liu,‡ Mouyi Weng,‡ Sibai Li, Xin Chen, Jianhang Cen, Jianshu Jie, Weiji Xiao, Jiaxin Zheng* and Feng Pan *

Received 19th August 2019,
Accepted 22nd October 2019

DOI: 10.1039/c9cp04591k

rsc.li/pccp

Titania is a widely used semiconductor due to its excellent optoelectronics and catalytic properties. Doping with other cations or anions by substitution of Ti or O is a common way to adjust the electronic structure of pristine TiO_2. Here, using *ab initio* calculations at the Heyd–Scuseria–Ernzerhof (HSE06) level, the substitution energy, formation energy and electronic structures of anatase TiO_2 doped with 40 kinds of elements including transition metals, alkali metals, alkaline earth metals, p-block metals, and nonmetals have been studied systematically. It is found that doping with most of these elements can narrow down the band gap of TiO_2, while in some doped systems, a recombination center induced by intermediate bands is also observed. Besides, for transition metal-doped TiO_2 systems, the electron spin state analysis of dopants and the doping level investigation reveal that a relatively high spin structure tends to be formed in Cr, Mn, Fe, Zn, Mo, Tc, Ru and Cd-doped TiO_2, and the doping levels of 4d-orbital transition metals are generally higher than those of 3d-orbital transition metals.

1. Introduction

In recent years, titania (TiO_2) has drawn much attention as a promising material for photocatalytic and photochemical reactions,[1–4] environmental purification,[5] water splitting applications[6,7] and transparent conducting oxides (TCOs).[8–10] However, pristine TiO_2 can only be excited by ultraviolet (UV) light radiation with the wavelength below 400 nm because of its large band gap (E_g = 3.20 eV for the anatase phase and 3.0 eV for the rutile phase).[11–15] In order to enhance its reaction efficiency, it is very important to narrow the band gap of TiO_2 and extend its optical absorption region to the visible and/or near infrared spectral region.[16,17] Doping is an effective method to adjust the electronic structure of TiO_2 and extend the functionalities of TiO_2 into the visible light region, and it is able to enhance the photovoltaic and photocatalytic efficiencies. Lots of experimental[4,18–74] and theoretical[4,32,75–87] efforts have been made to study the doping effects of transition metals, alkali metals, alkaline earth metals, p-block metals and nonmetals.

Nevertheless, nearly all the theoretical studies on the doping effect in TiO_2 were based on *ab initio* calculations at the LDA or GGA level. It is well known that standard DFT calculations including LDA[88] and GGA[89–91] underestimate the band gaps of semiconductors. LDA/GGA+U[92,93] can correct the band gap values effectively but relies on empirical parameters varying for different elements and different systems. Especially, in doped TiO_2 systems, there is no convincing method to determine the U value for the doped element. In many cases, the Hubbard U values are quite arbitrary. For the above reasons, the calculated results of doped TiO_2 systems by different groups using different U values are not comparable and even provide wrong predictions. The HSE06 functional[94–96] can improve the accuracy of the band gap calculation with standard parameters. These parameters have been proved to work well with the band gaps of common semiconductors.[95] Actually, the HSE06 functional has already been adopted to study the doping effect in TiO_2 in previous theoretical works.[97–100] However, due to the large computation cost of HSE calculation, the unit cells built for calculation in these works cannot be too large and the doping content is usually much higher than the practical content in experiments. For example, Tsai *et al.*[97] calculated the transition metal-doped TiO_2 using HSE06, and proposed an approach to screen $TiMO_2$ (M = transition metals) as the support materials of Pt applied in fuel cells. The doping concentration in their work is up to 25 at%. Moreover, all these works only concern certain specific systems, and a systematic accurate theoretical study on the doping effect of TiO_2 by HSE06 calculations is lacking. Given the above situation, it is worthwhile to conduct a systematic theoretical study on electronic structures of doped anatase TiO_2 by using the HSE06 functional, which can not only provide more accurate electronic structures for the doped systems but can also faciliate finding new physics and obtaining the general rule for the doping effect in TiO_2.

School of Advanced Materials, Peking University, Shenzhen Graduate School, Shenzhen 518055, China. E-mail: zhengjx@pkusz.edu.cn, panfeng@pkusz.edu.cn

† Electronic supplementary information (ESI) available. See DOI: 10.1039/c9cp04591k

‡ J. L. and M. W. contributed equally to the present paper.

In this work, we attempt to systematically study the electronic structures of anatase TiO_2 doped by 40 different kinds of elements including transition metals, alkali metals, alkaline earth metals, p-block metals and nonmetals at HSE06 level. Most of these elements have been doped in previous experimental works, such as V,[23,24,62,64,67] Cr,[61,63] Mn,[25,40] Fe,[51,52,69,70] Co,[60,68] Ni,[56] Cu,[58,59] Zn,[29,73] Y,[74] Zr,[19,20] Nb,[4,21] Mo,[71,72] Ru,[18,22] Rh,[55,57] Pd,[65,66] Ag,[53,54] Cd,[26] Li,[48–50] Na,[47] K,[47] Rb,[47] Be,[44] Mg,[42] Ca,[43] Sr,[45] Al,[34] Ga,[36] In,[35] Ge,[37,41] Sn,[38,39] Si,[33] C,[27,31] B,[28] N,[27,31,32] P[30] and S.[27,31] Based on the uniform parameters used in our calculation, electronic structures and doping effects between different doped systems are compared. Besides, the electron spin states of dopants for transition metal-doped TiO_2 and the relationship between the doping elements and the intermediate band levels have also been systematically investigated. We find that 4d-orbital transition metals tend to introduce a higher doping level to the doped systems than 3d-orbital transition metals, and nearly all the doping elements can reduce the band gap of TiO_2 and broaden the absorption spectrum. Our results provide guidelines on doping elements for designing photocatalytic devices based on anatase TiO_2 with high performance.

2. Computational method

We used density functional theory (DFT)[101] for all our calculations. In our structural relaxation steps, a $2 \times 2 \times 2$ supercell of TiO_2 with one doped atom is used, as shown in Fig. 1. This corresponds to a doping concentration of 6.250 at%. All our calculations are implemented in PWmat,[102,103] which runs on graphics processing unit (GPU) processors, and the NCPP-SG15-PBE pseudopotential[104,105] is used. Electron spin states have been considered before performing the structure optimization. After separately optimizing the structure for each plausible spin state, the lowest energy spin state was chosen for further calculations. Structure optimization is performed based on the generalized gradient approximation (GGA). The Perdew–Burke–Ernzerhof (PBE) exchange correlation[91] and a plane wave representation for the wave-function with a cutoff of 816 eV (60 Ryd) are used. The Brillouin zone was sampled by $4 \times 4 \times 3$ special k-points using the Monkhorst–Pack scheme[106] for structure optimization. The calculation will not finish until the force is less than 0.01 eV $Å^{-1}$ on each atom and the energy between two successive steps is less than 10^{-4} eV. In electronic structural calculations, a $4 \times 3 \times 3$ Monkhorst Pack k-point set was used for HSE06 self-consistent calculation and for DOS calculation. And the plane wave cutoff energy for wave-function used here is also 816 eV (60 Ryd). In HSE06, we have used the following standard parameters: $\alpha = 0.25$ and $\omega = 0.20$,[95,96] which work well in terms of correcting the band gaps of common semiconductors.

3. Results and discussion

3.1. Lattice constant and substitution energy and formation energy

Fig. 1(a) shows anatase TiO_2 with doped elements at Ti sites. Table 1 shows the lattice constant, substitution energy and

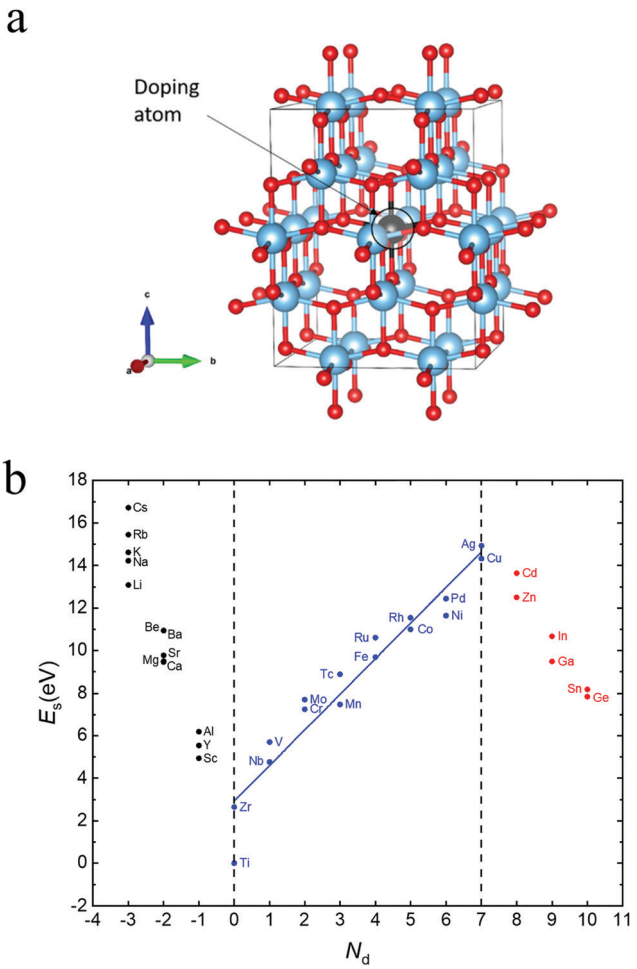

Fig. 1 (a) Anatase TiO_2 doped with elements, where red, blue and brown denote oxygen, titanium, and dopant atoms, respectively. The dopant atom replaces a titanium atom. (b) The relation between the substitution energy (E_s) and N_d, which denotes the difference of the number of valence electrons between dopant atom and metal Ti atom. The line is the fitted linear model based on the E_s of transition metal-doped systems. The slope is 1.67, the intercept is 2.93, and $R^2 = 0.93$.

formation energy for pristine anatase TiO_2 and all doped systems. Our calculated results of pristine TiO_2 are $a = b = 7.518$ Å and $c = 9.372$ Å, which are roughly consistent with the experimental results ($a = b = 7.568$, and $c = 9.515$ Å).[107,108]

Furthermore, to assess the relative stability of doped TiO_2 with different dopants, the substitution energy of the doped systems (E_s) is calculated. Considering that each dopant atom replaces a titanium atom in our calculations, as shown in Fig. 1(a), we can use the following equation to get substitution energies:

$$\begin{aligned} E_s &= E^{d}_{TiO_2} + E_{Ti} - E_d - E^{p}_{TiO_2} \\ &= \left(E^{d}_{TiO_2} - E_d\right) - \left(E^{p}_{TiO_2} - E_{Ti}\right) \end{aligned} \quad (1)$$

where $E^{d}_{TiO_2}$ and $E^{p}_{TiO_2}$ are the total energies of the doped system and pristine supercell anatase TiO_2, respectively; E_{Ti} and E_d are energies per atom for metal Ti and dopants, each in the form of

Table 1 Calculated properties of pristine and doped anatase TiO_2. The equilibrium lattice constants a, b and c, and the substitution energy (E_s) of doping and the formation energy (E_{fm}) of pristine and all the doped TiO_2 systems

Dopant	$a = b$ (Å)	c (Å)	E_s (eV)	E_{fm} (eV)
TiO_2	7.51796	9.37235	0	−149.0898
Sc	7.54009	9.39536	4.93509	−144.1547
V	7.51557	9.35689	5.695146	−143.3947
Cr	7.50464	9.37381	7.249112	−141.8407
Mn	7.50529	9.36325	7.473602	−141.6162
Fe	7.49259	9.41224	9.689646	−139.4002
Co	7.49804	9.3603	10.99778	−138.092
Ni	7.49973	9.36417	11.64079	−137.449
Cu	7.48743	9.37389	14.32101	−134.7688
Zn	7.52162	9.39073	12.49569	−136.5941
Y	7.55462	9.48507	5.537453	−143.5524
Zr	7.53711	9.45009	2.643256	−146.4466
Nb	7.54094	9.38412	4.758256	−144.3316
Mo	7.53704	9.37343	7.705243	−141.3846
Tc	7.53623	9.36741	8.877888	−140.2119
Ru	7.53503	9.36382	10.60493	−138.4849
Rh	7.53044	9.36515	11.54304	−137.5468
Pd	7.53278	9.37164	12.43474	−136.6551
Ag	7.52904	9.43462	14.92767	−134.1622
Cd	7.53689	9.50437	13.63303	−135.4568
Li	7.53332	9.31932	13.08565	−136.0042
Na	7.55708	9.38223	14.22519	−134.8646
K	7.55165	9.66129	14.62018	−134.4696
Rb	7.55456	9.71642	15.45534	−133.6345
Cs	7.5692	9.73576	16.72006	−132.3698
Be	7.48421	9.34548	10.94096	−138.1489
Mg	7.53546	9.35056	9.496281	−139.5935
Ca	7.55913	9.45962	9.456507	−139.6333
Sr	7.5495	9.65751	9.77512	−139.3147
Ba	7.55548	9.73782	10.93572	−138.1541
Al	7.50301	9.35399	6.186241	−142.9036
Ga	7.51959	9.37147	9.486099	−139.6037
In	7.54225	9.45852	10.67036	−138.4195
Ge	7.49761	9.40643	7.842246	−141.2476
Sn	7.5306	9.45448	8.182663	−140.9072
Si	7.47902	9.37175	4.988594	−144.1012
C	7.58024	9.25395	14.19592	−134.8939
B	7.47631	9.3124	11.56507	−137.5248
N	7.48757	9.3606	19.88957	−129.2003
P	7.47929	9.34675	8.096238	−140.9936
S	7.50964	9.35944	12.59627	−136.4936

its own most stable elementary substance, respectively. The substitution energies of all the doped systems are positive, which indicates that the doped impurities are in metastable states at the local minima, and thus all the doped systems are not as thermodynamically stable as pristine anatase TiO_2. This is easy to understand, because all the substitutional doping reactions are not spontaneous processes. But, it is worth noting that the positive substitution energy does not mean that the doped system itself is not thermodynamically stable. To investigate the intrinsic thermodynamic stability of doped TiO_2 consisting of one atom doped into the anatase TiO_2 host, we further calculated the formation energies of each doped TiO_2 system. The formation energies of pristine anatase TiO_2 (E^p_{fm}) and doped systems (E^d_{fm}) can be calculated by eqn (2) and (3), respectively:

$$E^p_{fm} = E^p_{TiO_2} - 16 \times E_{Ti} - 32 \times E_O \quad (2)$$

$$E^d_{fm} = E^d_{TiO_2} - 15 \times E_{Ti} - 32 \times E_O - E_d \quad (3)$$

where E_O refers to energy per atom in O_2 gas, which is the most stable elementary form of oxygen under ambient conditions. The formation energy of the doped systems (E^d_{fm}) can also be calculated by eqn (4), which is obvious if we add eqn (1) to (2):

$$E^d_{fm} = E_s + E^p_{fm} \quad (4)$$

From Table 1, we can see that the formation energy values of all the doped systems (E^d_{fm}) are negative, which is evident because the substitution energy (E_s) values of all the doped systems are much smaller than the absolute value of the formation energy of pristine anatase TiO_2 (E^p_{fm}), which is calculated as −149.09 eV. The negative formation energy indicates that each doped system itself is thermodynamically stable, consistent with what we mentioned above that most of these elements have been doped in previous experimental works,[4,18–74] which proves that all these doped systems are at least thermodynamically stable enough to exist.

In addition, roughly speaking, for metal-doped TiO_2 systems, the substitution energy (E_s) shows a positive correlation with N_d, which refers to the difference of the number of valence electrons between dopant atom and metal Ti atom, as Fig. 1(b) shows. Especially for the transition metal (from group 4 to group 11)-doped TiO_2 systems, E_s and N_d are approximately linearly related as eqn (5) shows:

$$E_s = 1.67N_d + 2.93 \quad (5)$$

The slope, the intercept and the R^2 values of the fitting line are 1.67, 2.93 and 0.93, respectively. This linear relationship can be attributed to the fact that the energy increment is proportional to the amount of electrons introduced, which is roughly similar to adding electrons to the pristine TiO_2 system directly.

3.2. The electron spin state analysis of the dopant atom

Compared with the pristine TiO_2 system, each doped system may have extra valence electrons or lack valence electrons, except for the Zr-doped system (because the N_d of Zr equals zero). These relatively extra valence electrons may be in different spin states. For example, when $N_d = 3$ (such as Mn), the relatively extra 3 valence electrons can be in 2 different spin states: three electrons are all spinning upwards (or downwards), or two electrons are spinning upwards (or downwards) and one electron is spinning downwards (or upwards). If we use N_s to denote the difference between the number of spin up extra valence electrons and the number of spin down extra valence electrons, then these two different situations can be described as $N_s = 3$ or $N_s = 1$, and the two different spin states can be denoted as "spin3" and "spin1", respectively. We call the "spin1" state the low spin state. In other words, the low spin state refers to the state in which N_s is the smallest.

The electron spin state is very important in the calculations, as it can severely affect the calculated properties for the system. For example, different electron spin states of a dopant atom can cause different calculated E_s values, especially for transition metal dopants, because all the transition metal elements have d-orbitals, and most d-orbital metal-doped TiO_2 systems have

spin polarization. Thus, it is very necessary to do the electron spin state analysis through which we can find the spin state in which the E_s of the system is the lowest, and conversely, by evaluating the value of E_s, we can investigate the spin tendency of the electrons of the doped atom.

What needs to be emphasized is that the spin state we discussed in this context refers to the spin state of the relatively extra valence electrons introduced by the dopant. However, since pristine TiO_2 is a spin-free system in which the electrons of Ti and O are each paired, the analysis of the spin state of the relatively additional electrons introduced by the impurity atom is equivalent to analyzing the electronic spin state of the entire doped system. Here, taking a transition metal-doped system as an example, let us discuss the relations between the spin state of d-orbital electrons and the E_s of the doped system. Fig. 2(a) shows the relations between the E_s in different spin states and the N_d, which are similar to what Fig. 1(b) shows, and the difference is that Fig. 2 also shows the influence of spin state on E_s. The dopants with $N_s \geq 2$ have 2 or 3 different spin structures, which corresponds to the relative extra valence electrons in different spin states, and the different spin states can be characterized by the N_s. Therefore, we name these different spin structures as the low spin structure, middle spin structure and high spin structure, respectively, which correspond to the smallest N_s, the middle N_s and the largest N_s, respectively.

We can find the lowest E_s for each dopant from Fig. 2(a); yet, the spin tendency of each dopant is not obvious in Fig. 2(a). Hence, we plotted Fig. 2(b) by taking the E_s of the low spin state as the baseline for each dopant. For the convenience of description, we introduce ΔE_s, which is defined in eqn (6), as the ordinate.

$$\Delta E_s = E_s - E_s^l \quad (6)$$

where E_s^l denotes the substitution energy of doped TiO_2 with dopant atom in low spin structure; so, for each dopant element, its ΔE_s is zero when it is in its low spin structure.

The spin tendency can be clearly described by evaluating whether the value of ΔE_s is positive or negative. Fig. 2(b) shows some regular patterns for d-orbital metal dopants: for the dopants whose N_d is equal to 2, 3, 4, or 8, their ΔE_s is negative, so they tend to have a relatively high spin structure (middle spin structure) in doped TiO_2. These dopants are 3-d-orbital metals, Cr, Mn, Fe, and Zn, and 4-d-orbital metals, Mo, Tc, Ru, and Cd. While for the dopants whose N_d is equal to 5, 6, or 7, their ΔE_s is positive, so they tend to have a low spin structure in doped TiO_2. These dopants are 3-d-orbital metals, Co, Ni, and Cu, and 4-d-orbital metals, Rh, Pd, and Ag.

This is consistent with the results of the crystal field theory. In anatase TiO_2, the Ti atom is at the center of an octahedron composed of O atoms, and the doping atom replaces the Ti atom, thereby also filling in the octahedron of O. According to the orbital arrangement rule of the octahedral crystal field (the energy of the three t_{2g} orbitals is lower, and the energy of the two e_g orbitals is higher), when N_d is equal to 2, 3, 4 or 8, a relatively high spin arrangement is taken; and when N_d is equal to 5, 6 or 7, a low spin arrangement is taken. In particular, Fig. 2(b) shows that when N_d is equal to 3 or 6, the absolute value of ΔE_s is the largest. This corresponds to the states where the three t_{2g} orbitals are half-filled and fully filled, respectively, at which time the energy is at a minimum. Peng *et al.*[78] studied the magnetic properties of 3d transition metal-doped anatase TiO_2 by first-principles calculations, and they reported similar results to ours. Our new results show that the 4d transition metal-doped anatase TiO_2 possesses similar magnetic properties.

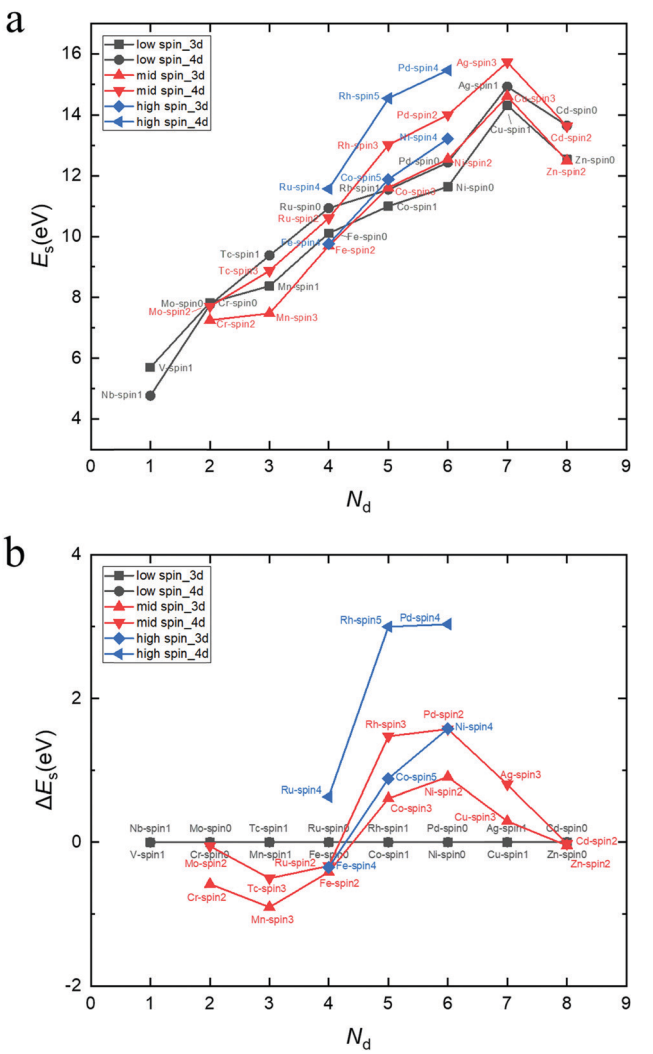

Fig. 2 The electron spin state of transition metal dopant atom and its influence on the substitution energy (E_s). (a) The relations between ΔE_s and N_d. (b) The relations between E_s and N_d. The abscissa N_d is the same as in Fig. 1(b). E_s denotes the difference between E_s and E_s^l (the substitution energy of doped TiO_2 with dopant atom in low spin structure). The low spin structure means that the N_s (the difference between the number of spin up extra valence electrons and the number of spin down extra valence electrons) is the smallest. The term "spin0" refers to $N_s = 0$, and "spin1" refers to $N_s = 1$, and so on. For the dopants whose N_d is equal to 2, 3, 4, or 8, their ΔE_s is negative, so they tend to have a relatively high spin structure (middle spin structure) in doped TiO_2, while for the dopants whose N_d is equal to 5, 6, or 7, their ΔE_s is positive, and so they tend to have a low spin structure in doped TiO_2.

In fact, the electron spin states have already been considered in all the calculations, so all the data (except Fig. 2) are the final results obtained by the calculations performed with the optimum spin state parameters, which makes the doped systems the most thermodynamically stable.

3.3. Electronic structures

The projected density of states (PDOS) of pristine anatase TiO_2 is shown in Fig. 3 (labeled with "Ti"). It can be seen that the valence band (VB) and conduction band (CB) are mainly composed of O-2p and Ti-3d-orbitals, respectively. The band structure information can be seen in the ESI.† The band gap of pristine anatase TiO_2 is estimated to be 3.59 eV, which is roughly consistent with the experimental value of 3.2 eV.[11–14]

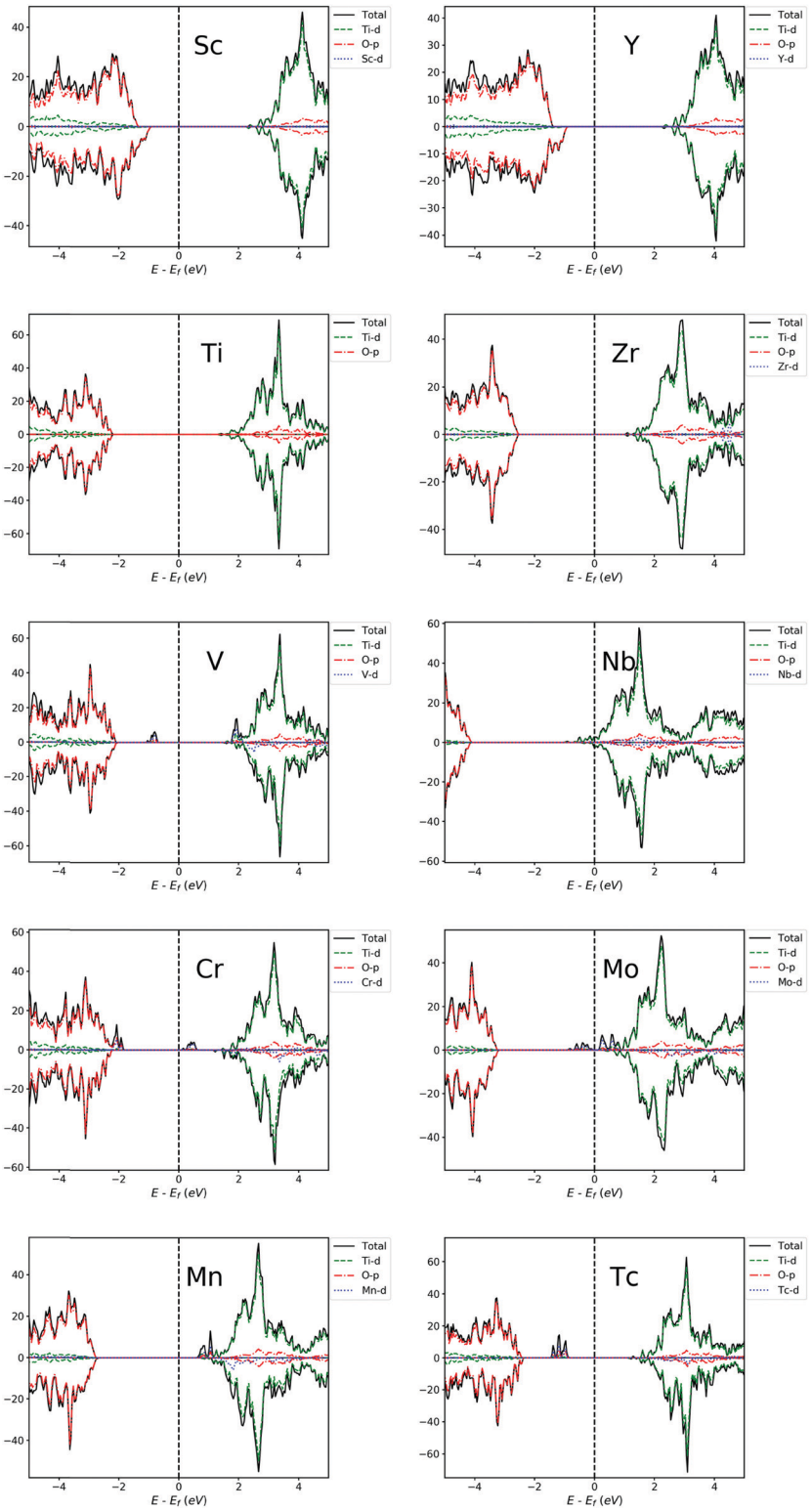

Fig. 3 PDOS of Sc, V, Cr, Mn, Y, Zr, Nb, Mo and Tc-doped TiO_2 systems and pristine TiO_2. The Fermi level is set at zero energy.

We also estimated the position of the conduction band minimum (CBM) and valence band maximum (VBM) described by *k*-point coordinates, and the results are presented in Table S1 (ESI†). It turns out that the band gap of pristine anatase TiO_2 presents an indirect nature, which is consistent with previous theoretical[109,110] and experimental[111,112] results. However, the direct band gap is estimated to be 3.63 eV, which is only 0.4 eV larger than the indirect band gap. Therefore, the band gap of pristine anatase TiO_2 can be almost recognized as a direct gap if we judge only from the band structure diagram (Fig. S1, ESI†).

3.3.1 Transition metal-doped TiO_2 systems. Fig. 3 and 4 show the PDOS of transition metal-doped TiO_2 systems. For Sc and Y-doped TiO_2 systems, because the valence states of Sc and Y (+3) are lower than Ti (+4), the O-2p-orbital has an unpaired electron, leading to asymmetry of the PDOS. Besides, it can be found that the Fermi level shifts downwards to the top of the VB compared to the pristine TiO_2, indicating that each Sc or Y dopant offers a hole as charge carrier in TiO_2, and in consequence, the concentration of charge carriers is increased, which is beneficial to the improvement of photocatalytic efficiency. This is in agreement with the experimental results obtained by Zhao *et al.*[74] that 3 at% Y-doping in anatase TiO_2 applied in dye-sensitized solar cells caused the photocurrents to improve vastly (from 13.2 to 15.74 mA cm^{-2}) due to the increment of concentration of charge carriers. For the Zr-doped TiO_2 system, it is found that the PDOS is almost the same as pristine TiO_2, which is consistent with the previous reported GGA results[19] that the DOS around the Fermi level remained unchanged and no defect level appeared within the gap in the 6.25 at% Zr-doped anatase TiO_2. Considering that both Zr and Ti are IV-B group transition metals and have the same 4 valence electrons, it is easy to understand that their electronic structures are nearly the same. The features of PDOS of Sc, Y, and Zr-doped TiO_2 systems are basically consistent with the previous reported GGA+*U* results.[76,79] However, there are differences in the position of the Fermi level. The Fermi level has shifted into the VB in their GGA+*U* results, but it still remains in the band gap in our HSE06 results. The Fermi level located in the VB means that the doped system has already somehow behaved like a metal, which is not reasonable for the substitutional doping, especially for Zr, which has the same valence electrons as Ti. This demonstrated that our HSE06 results are more reasonable and more accurate.

For other transition metal-doped TiO_2 systems, the number of valence electrons of the dopant is more than that of Ti, and therefore, it is interestingly found that the defect states usually appear in the forbidden gap of the pristine TiO_2 to form intermediate bands (IBs). Thus, the intrinsic forbidden gap is divided into two or many sub-gaps by the presence of such IBs. On one hand, the intermediate states can be a stepping stone to help valence electrons get excited into the CB under the illumination of low energy photons, which will promote the efficiency of optical absorption of low energy photons. On the other hand, the IBs would also act as recombination centers, which make electron and hole recombination much easier. The probability of excitation or recombination depends on the energy difference between VB and IBs or CB and IBs. Usually, the deep level defect states easily become recombination centers, and the shallow defect states, in contrast, are beneficial for charge separation. In addition, for most of the transition metal dopants, the defect states of the doped systems are mainly composed of d-orbital states of dopants, except for Cu, Ag, Zn and Cd (Fig. 3 and 4), because these metal dopants possess a fully occupied d-orbital (d^{10}). Especially for the systems doped by Zn and Cd (with a stable electron configuration of $d^{10}s^2$), the defect states with no proportion of d-orbital states from dopants are totally composed of O-2p states of the host (Fig. 4).

For each Zn, Cd, Ru, Mn, Nb, Mo or Pd-doped TiO_2 system, the PDOS from Fig. 3 and 4 shows that all the defect states are nearly at the top of the VB (Zn, Ru and Cd) or the bottom of the CB (Mn, Nb, Mo, Ru and Pd), forming the tail of the VB or CB, which can reduce the band gap. The reduction of band gap can extend its range of optical absorption region to the visible light region, which is beneficial to the improvement of optical absorption efficiency. Thus, doping these transition metals can enhance the photocatalytic efficiency. For Nb-doped TiO_2, the Fermi level moves into the CB, which was also reported from previous GGA+*U* calculations.[4,76,79] This means that the electrical conductivity of Nb-doped TiO_2 will be very excellent because of the existence of free electrons in the CB, which was confirmed by Yang *et al.*[4] through their combined theoretical and experimental work. Therefore, the photocatalytic efficiency of Nb-doped TiO_2 can be promoted vastly by an extended free carrier absorption of visible light and effective charge transfer. In addition, the band structure information (ESI†) reveals that Mo and Cd doping can change the type of band gap, *i.e.* turning an indirect band gap into a direct one, which is also beneficial for the optical absorption process and will improve the photocatalytic efficiency. These conclusions are in agreement with the previous experimental reports that doping Zn,[29,73] Ru,[18,22] Cd,[26] Mn,[25,40] Nb,[4,21] and Mo[113] can effectively reduce the band gap and thus can obtain visible light responsive TiO_2 with finally enhanced photocatalytic efficiency.

For each V, Cr, Fe, Co, Tc, Rh or Ag-doped TiO_2 system, it can be seen from Fig. 3 and 4 that parts of the IBs are integrated with the VB or CB and thus reduce the band gap, while the other parts of the IBs are located away from the VBM or CBM, dividing the intrinsic forbidden gap into two parts. The reduction of band gap for all these doped systems has been experimentally reported, such as those for V,[64,67] Cr,[61] Fe,[52] Co,[60] Rh[57] and Ag.[54] However, the reduction of band gap only means that the spectral activity is enhanced, while the eventual photocatalytic efficiency may not be improved because of the existence of recombination centers. For V and Tc-doped TiO_2 systems, the energy difference between VBM and IB minimum is much smaller than the energy difference between CBM and IB maximum, so the probability for a hole in the VB to pump up into the IB will be larger than the probability for an electron in the CB to combine with a hole in the IB. This is consistent with previous experimental results[64,67] that V doping enhanced the photocatalytic activity under visible light irradiation. While for Cr, Fe, Co and Ni-doped TiO_2 systems, the IBs are closer to the CBM than to the VBM, indicating a larger

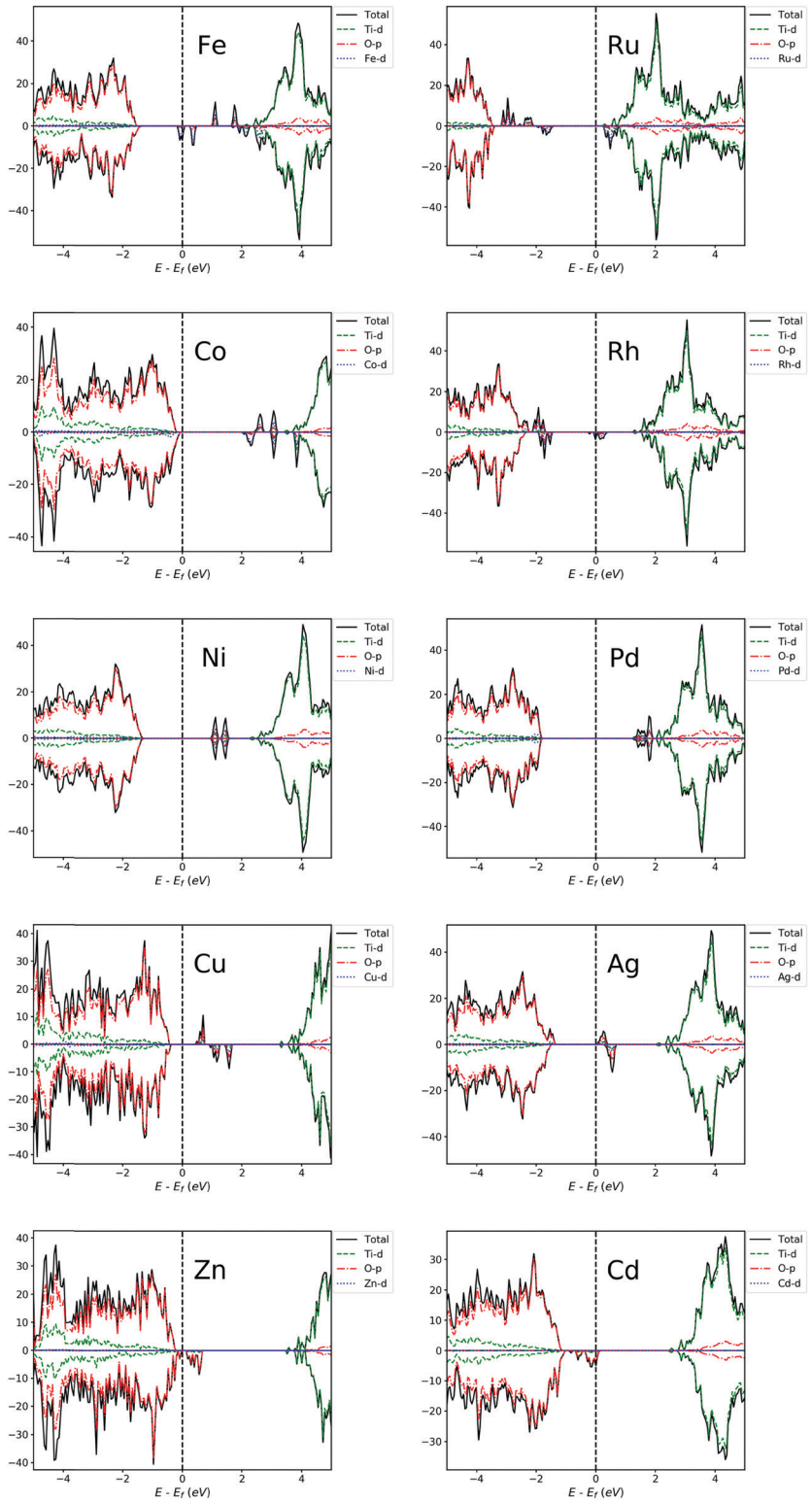

Fig. 4 PDOS of Fe, Co, Ni, Cu, Zn, Ru, Rh, Pd, Ag and Cd-doped TiO_2 systems. The Fermi level is set at zero energy.

probability for an electron in the CB to combine with a hole in the IB. Especially for Fe and Co-doped systems, the IBs are much closer to the CBM, so the photocatalytic performance of Fe or Co-doped TiO_2 will not be very good. This is in agreement with previous experimental results by Li *et al.*[52] that although the absorbing band edge has moved to the visible range after Fe doping into TiO_2, the photocatalytic activity is lower than that of the un-doped TiO_2. Besides, E. B. Gracien *et al.*[114] experimentally investigated the photocatalytic activity of Mn, Cr and Co-doped TiO_2, and they found that the photocatalytic efficiency of

Co-doped TiO_2 is worse than that of Cr or Mn-doped TiO_2 and Mn doping gives the best enhancement, consistent with our theoretical results. As for Cu, Rh and Ag-doped TiO_2 systems, their IBs are in the middle of the band gap, which introduces a deep level recombination center. Therefore, despite the reduction of band gap, doping these elements would not improve the photocatalytic performance vastly, which is confirmed by the experimental results by Mahlambi *et al.*[115] They reported that Ag, Co, Ni and Pd-doped TiO_2 exhibited photo activity under solar light irradiation, but the photocatalytic activity of the Ag-doped TiO_2 is almost as bad as that of the Co or Ni-doped TiO_2, and that of the Pd-doped TiO_2 is the best.

Peng *et al.*[78] reported their first-principles study on the electronic structures of anatase TiO_2 doped with 3d transition metals (V, Cr, Mn, Fe, Co and Ni). There are also IBs appearing in the band gap for most of the systems doped by these elements in their results, which is consistent with ours. However, because they used the LDA type exchange–correlation functional and without the Hubbard U parameter, the position of the IBs is different from ours. In general, because their LDA band gap is too small, many IBs are connected together, like being squeezed, especially for Fe and Co-doped systems, while most IBs are separated in our HSE06 results. Besides, there are more IBs in their results because their doping concentration is 12.5 at%, which is twice that of ours. For example, in their PDOS of the Cr-doped system, the integral area of IBs is quite large, even comparable to the CB or VB, and more importantly, the three t_{2g} states are located away from the VBM and are not clearly separated. By contrast, it can be seen from our Fig. 3 that the integral area of IBs for the Cr-doped system looks relatively small, and it is not comparable to the CB and VB. More importantly, Fig. 3 and 5 show that for Cr-doping, the splitting of two occupied t_{2g} (d_{xz} and d_{yz}) states and one unoccupied t_{2g} (d_{xy}) state has been clearly depicted by the HSE06 method; and compared with their LDA result, the two d_{xz} and d_{yz} states in our HSE06 result have been shifted down to the VBM and are connected to it. The splitting of three t_{2g} states for the Cr-doped TiO_2 system has also been reported in the GGA+U study by Yang *et al.*[116] However, in their GGA+U result, the two down shifted d_{xz} and d_{yz} states are still a little bit away from the VBM, revealing that the splitting of d_{xz} (d_{yz}) and d_{xy} states for Cr-doped TiO_2 in GGA+U calculations is not as strong as that in HSE06 calculations.

Most of the doping levels in the doping system are introduced by valence electrons. Since the valence electrons of all the transition metals are mainly d-orbital electrons, for transition metal-doped systems, the doping levels are mainly determined by the d-orbitals of the dopant atoms (except for Zn and Cd-doped system), as confirmed in Fig. 3 and 4. After a careful analysis of the doping level of transition metals, we found some rules. In order to make these rules clearer, we plot the PDOS of the d-orbitals of dopant atoms separately in Fig. 5. For the sake of comparison, the transition metals were divided into many pairs, such as V–Nb, Cr–Mo, Mn–Tc *etc.* In each pair, one element comes from a 3d-orbital, another from a 4d-orbital, and both elements have the same N_d. By comparing the two elements in each pair, it is easy to find that 4d-orbital transition metals tend to introduce a higher doping level to the doped systems than 3d-orbital transition metals, just as Fig. 5 shows. Besides, for each pair, the Fermi level of the 4d-orbital metal-doped system is generally higher than that of the 3d-orbital metal-doped system (except for the Mn–Tc pair). These rules indicate that compared with 3d-orbital dopant atoms, the impurity ionization energy of 4d-orbital dopants is generally smaller, meaning that the 4d-orbital electrons are more easily ionized than 3d-orbital electrons in the doped TiO_2 systems.

3.3.2 Alkali or alkaline earth metal-doped TiO_2 system. The PDOS of alkali/alkaline earth metal-doped TiO_2 is shown in Fig. 6, from which we can see that the intermediate energy states also appear in the forbidden gap of the pristine TiO_2. But, for alkali/alkaline earth metal-doped TiO_2, the intermediate states are mainly composed of O-2p-orbitals, which is very different from transition metal-doped TiO_2.

For alkali metal-doped TiO_2 systems, we can see that the VB moves towards the Fermi level, indicating the increment of concentration of charge carriers and the slight reduction of band gap. It can be seen from Fig. 6 that from Li to Cs, the position of IBs is roughly getting further away from the VBM, making it easier for them to become a recombination center, and thus, the beneficial effects of doping get worse and worse. This is in agreement with previous experimental results by Bessekhouad *et al.*[48] and Yang *et al.*[47] The former investigated the photocatalytic efficiency of Li, Na and K-doped TiO_2 and found that the Li-doped system exhibits the best photocatalytic performance among the three. The latter reported that the order of photocatalytic performance for degradation from better to worse is Na > K > Rb. In addition, the lower band gap and photocatalytic activity under sunlight or visible irradiation have been experimentally reported for Li-doped TiO_2.[46,50]

For alkaline earth metal-doped TiO_2 systems, the result is similar to alkali metal-doped TiO_2 systems, also with the Fermi level shifted towards the VBM and a slightly reduced gap. From Fig. 6, it can be seen that the position of IBs is roughly getting deeper into the gap from Be to Ba, which makes it easier for them to become recombination centers. Hence, roughly speaking, the beneficial effects of Be, Mg and Ca-doping are more obvious. Behnajady *et al.*[42] reported that their experimental results showed a lower band gap energy and a red shift of optical absorption for the Mg-doped anatase TiO_2, and Mg-doping ultimately caused the photocatalytic activity of anatase to improve significantly. The enhanced photocatalytic activity has also been experimentally reported for Be-doping[44] and Ca-doping.[43] In addition, the band structure information (ESI†) indicates that Be, Mg and Ca doping can obtain a direct band gap. Therefore, the beneficial effects of doping these elements will be more evident.

3.3.3 P-block metal-doped TiO_2 systems. Fig. 7 shows the PDOS of the P-block metal-doped TiO_2 systems. It can be seen that there are no IBs appearing in the intrinsic forbidden gap except for the Al-doped system. Due to the same number of valence electrons for III-A group metals and III-B group metals,

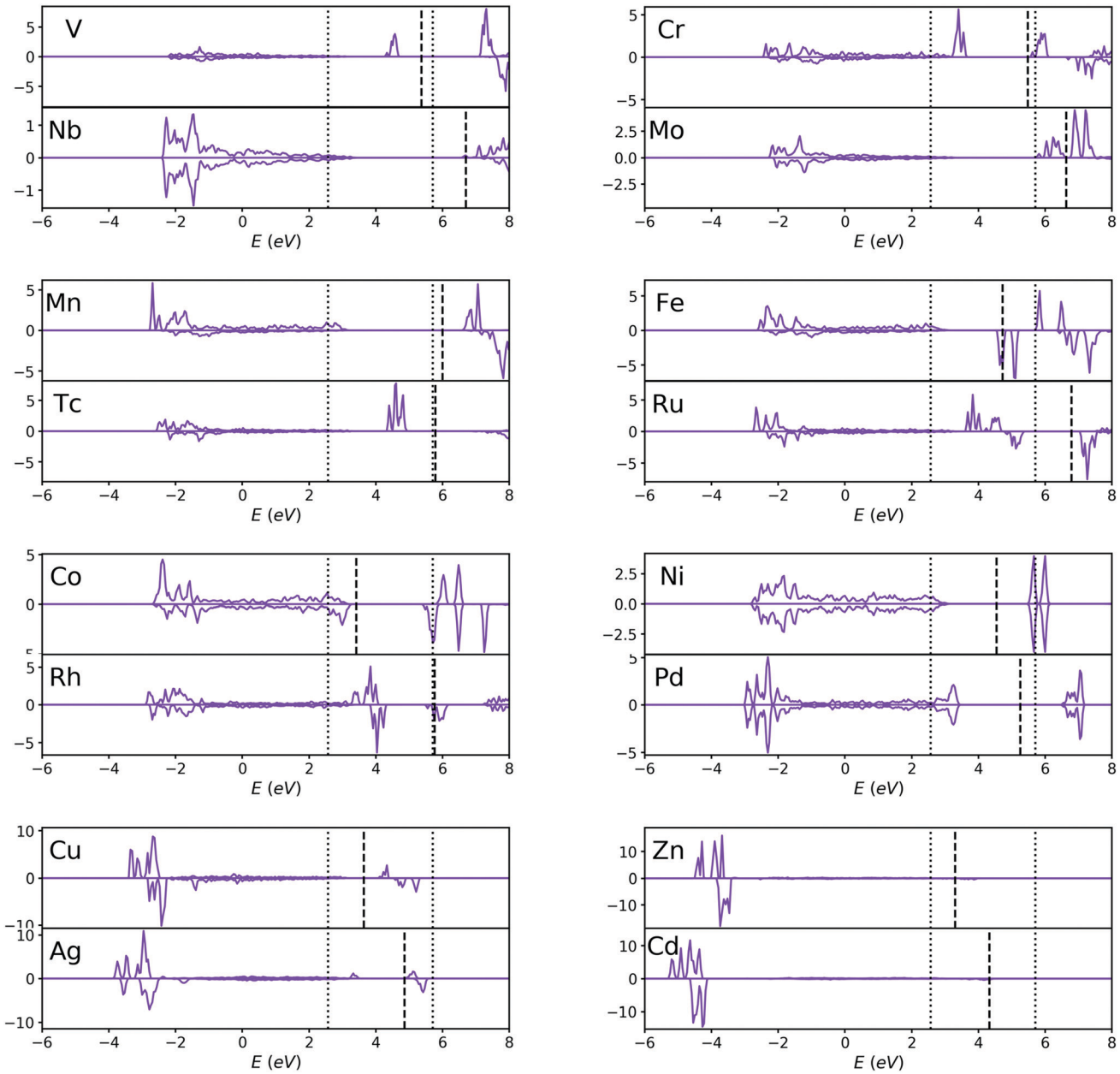

Fig. 5 PDOS of the d-orbitals of dopant atoms for V, Cr, Mn, Fe, Co, Ni, Cu, Zn, Nb, Mo, Tc, Ru, Rh, Pd, Ag and Cd-doped TiO_2 systems. The dotted lines are the VBM and CBM of pristine TiO_2 instead of doped TiO_2, and the dashed lines are the Fermi levels of each doped system. The two elements with the same N_d are classified as one pair. For each pair, 4d-orbital transition metals tend to introduce a higher doping level to the system than 3d-orbital transition metals, and the Fermi levels of 4d-orbital metal doped systems are generally higher than those of 3d-orbital metal doped systems (except for Mn–Tc pairs).

the characters of PDOS of Al, Ga and In (III-A group metal)-doped TiO_2 systems are similar to those of Sc and Y (III-B group metal)-doped TiO_2 systems. However, the difference is that Al, Ga, and In-doped TiO_2 systems all possess a direct band gap (see ESI†), so the beneficial effects of this element-doping will be better than that of Sc and Y-doping. The Fermi level shifts down towards the VBM and reduces the band gap slightly. The p-type doping of these metals offer holes as charge carriers, resulting in the increment of carrier concentration. The increased carrier concentration and thus enhanced electrical conductivity have been experimentally reported for In-doped anatase TiO_2 by Zhao *et al.*[35] Besides, Shirley *et al.*[87] investigated the electronic and optical properties of Al-doped anatase TiO_2 by first-principles calculations with many different kinds of models considered and reported that the model of one Ti atom substituted by an Al atom exhibits a reduction of band gap and a shift of absorption towards long wavelengths, which is also consistent with our calculations. However, their results calculated by using the PBE functional also showed that the model of

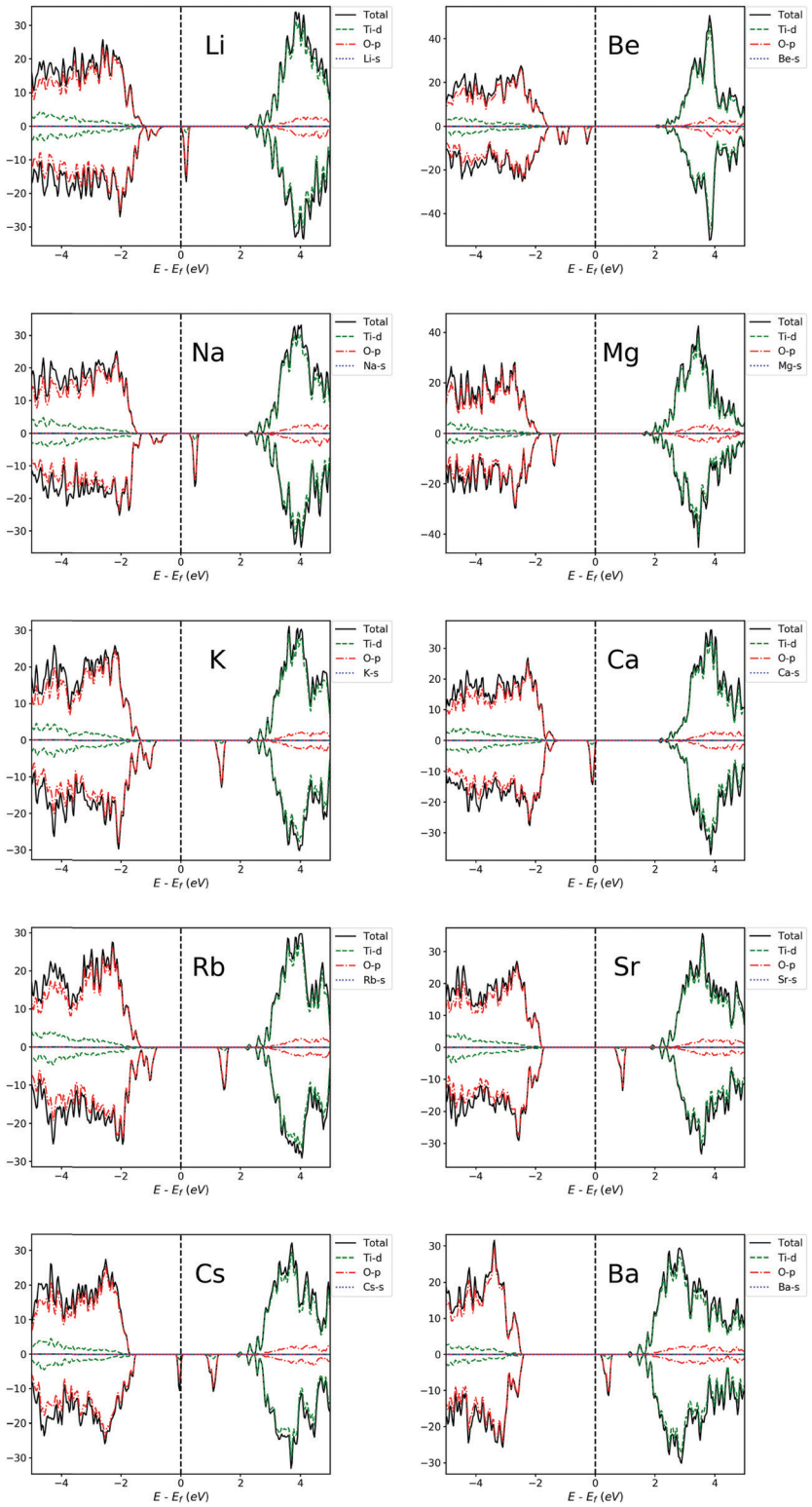

Fig. 6 PDOS of Li, Na, K, Rb, Cs, Be, Mg, Ca, Sr and Ba-doped TiO_2 systems. The Fermi level is set at zero energy.

one Ti atom replaced by an Al atom yielded a conductor for Al-doped TiO_2, which is different from our HSE06 result. This once again demonstrates that the HSE06 functional provides higher accuracy for prediction of electronic structures. Similarly, the PDOS of Ge and Sn-doped TiO_2 systems is similar to those of the Zr-doped TiO_2 system and pristine TiO_2, owing to the same number of valence electrons for metals from IV-A group (Ge and Sn) and IV-B group (Zn and Ti). Thus, the PDOS and band gap nearly remain unchanged for these metal-doped systems.

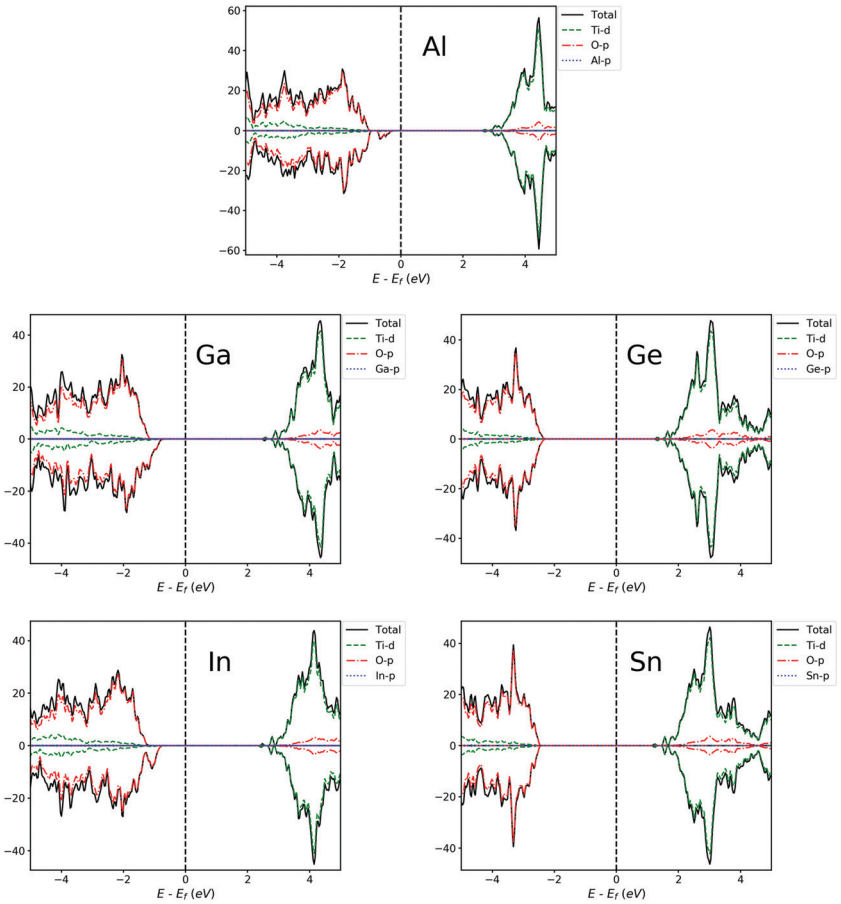

Fig. 7 PDOS of Al, Ga, In, Ge and Sn-doped TiO_2 systems. The Fermi level is at zero energy.

3.3.4 Nonmetal-doped TiO_2 systems. The PDOS of nonmetal-doped TiO_2 systems is shown in Fig. 8. For B, N and S-doped TiO_2 systems, the Fermi level shifts towards the VBM, and the IBs closer to the VBM also appear in the intrinsic gap, which results in a reduction of the band gap. While for P-doped systems, the Fermi level moves towards the CBM, and no IBs appear in the intrinsic gap. The reduction of band gap and redshift of absorption for B, N and S-doped anatase TiO_2 have been theoretically[81,82] and experimentally[27] reported. For example, Han *et al.*[82] performed DFT calculations at the GGA+*U* level for N-doping with a Ti atom replaced by a N atom, and they obtained a similar result with the IBs also appearing in the gap and above the VB and a reduced band gap. Harb *et al.*[81] calculated S-doped TiO_2 with many different doping models considered using the HSE06 functional and their result for the model of a Ti atom substituted by a S atom is consistent with ours. In addition, Yang *et al.*[80] reported a similar computational result for B-doped anatase TiO_2 with a Ti atom substituted by a B atom. However, because the exchange–correlation functional that they used is a GGA type and without the Hubbard U parameter, the defect states induced by doping are near the VB in their calculated DOS, whereas in our HSE06 result, the defect states are located away from the VB and the IBs form in the intrinsic gap. In addition, a direct band gap for the B and P-doped TiO_2 systems is suggested by the band structure information (ESI†), so the doping effects of these two elements will be better. As for C and Si-doped TiO_2 systems, similar to those of Ge and Sn, because of the same number of valence electrons for elements from IV-A group and IV-B group, the PDOS and band gap for these doped systems are nearly the same as those of the Zr-doped TiO_2 system and pristine TiO_2. However, the band structure information (ESI†) reveals that the band gap of C and Si-doped TiO_2 systems shares a direct nature, which is different from Ge, Sn and Zr-doping. Therefore, even though the change of the band gap size is not evident, the change of the band gap type from indirect to direct makes the beneficial doping effects of C and Si-doped TiO_2 systems better than those of Ge, Sn and Zr-doped TiO_2 systems.

4. Conclusions

In summary, anatase TiO_2 doped with 40 kinds of elements has been systematically studied by using first-principles calculation at the HSE06 level. The results show that doping with most of these elements can reduce the band gap. However, in some doped systems, the introduced intermediate bands may act as recombination centers and can lower the photocatalytic efficiency. Based on the effect of doping on photocatalytic performance, the doped systems can be

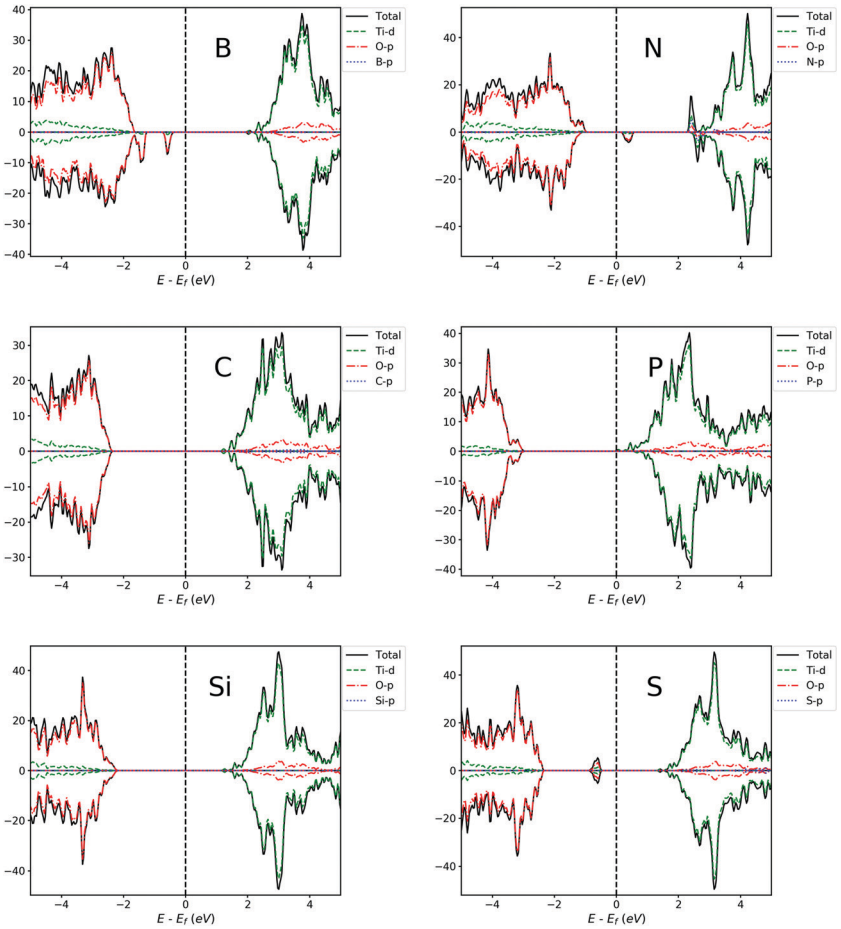

Fig. 8 PDOS of B, C Si, N, P and S-doped TiO_2 systems. The Fermi level is set at zero energy.

divided into three types: (1) Sc, Y, Zn, Ru, Cd, Mn, Nb, Mo, Pd, V, Tc, Li, Na, Be, Mg, Ca, Al, Ga, In, B, N, S and P-doping can reduce the band gap and enhance the photocatalytic efficiency for anatase TiO_2. (2) For Cr, Fe, Co, Ni, Cu, Rh, Ag, K, Rb, Cs, Sr, and Ba-doped TiO_2 systems, the introduced IBs will make the photocatalytic efficiency lower. (3) For Zr, Ge, Sn, C and Si-doped TiO_2 systems, doping has little effect.

For transition metal-doped systems, E_s and N_d are approximately linearly related. The electron spin state analysis of the dopant atom for transition metal-doped systems shows that Cr, Mn, Fe, Zn, Mo, Tc, Ru and Cd-doped TiO_2 tends to have a relatively high spin structure; while Co, Ni, Cu, Rh, Pd and Ag-doped TiO_2 tends to have a low spin structure. Besides, 4d-orbital transition metals tend to introduce a higher doping level to doped systems than 3d-orbital transition metals, and the Fermi level of 4d-orbital metal-doped TiO_2 is generally higher than that of 3d-orbital metal-doped TiO_2, which indicates that the 4d-orbital electrons are more easily ionized than 3d-orbital electrons in doped TiO_2 systems.

Conflicts of interest

There are no conflicts to declare.

Acknowledgements

This study was financially supported by the National Key R&D Program of China (2016YFB0700600), the National Natural Science Foundation of China (No. 21603007 and 51672012), the Soft Science Research Project of Guangdong Province (No. 2017B030301013), Shenzhen Science and Technology Research Grant (No. JCYJ20150729111733470 and JCYJ20151015162256516), and the New Energy Materials Genome Preparation & Test Key-Laboratory Project of Shenzhen (No. ZDSYS201707281026184).

References

1 S. U. M. Khan, M. Al-Shahry and W. B. Ingler, *Science*, 2002, **297**, 2243–2245.
2 X. Chen, L. Liu, P. Y. Yu and S. S. Mao, *Science*, 2011, **331**, 746–750.
3 S. N. Habisreutinger, L. Schmidt-Mende and J. K. Stolarczyk, *Angew. Chem., Int. Ed.*, 2013, **52**, 7372–7408.
4 X. Yang, Y. Min, S. Li, D. Wang, Z. Mei, J. Liang and F. Pan, *Catal. Sci. Technol.*, 2018, **8**, 1357–1365.
5 S. Ikezawa, H. Homyara, T. Kubota, R. Suzuki, S. Koh, F. Mutuga, T. Yoshioka, A. Nishiwaki, Y. Ninomiya,

M. Takahashi, K. Baba, K. Kida, T. Hara and T. Famakinwa, *Thin Solid Films*, 2001, **386**, 173–176.
6 A. J. Cowan, J. Tang, W. Leng, J. R. Durrant and D. R. Klug, *J. Phys. Chem. C*, 2010, **114**, 4208–4214.
7 A. J. Bard and M. A. Fox, *Acc. Chem. Res.*, 1995, **28**, 141–145.
8 T. Hasegawa, G. Kinoda, K. Inaba, T. Hitosugi, Y. Hirose, Y. Yamamoto, Y. Furubayashi and T. Shimada, *Appl. Phys. Lett.*, 2005, **86**, 252101.
9 D. S. Bhachu, S. Sathasivam, G. Sankar, D. O. Scanlon, G. Cibin, C. J. Carmalt, I. P. Parkin, G. W. Watson, S. M. Bawaked, A. Y. Obaid, S. Al-Thabaiti and S. N. Basahel, *Adv. Funct. Mater.*, 2014, **24**, 5075–5085.
10 X. Yang, M. J. Zhang, Y. Min, M. Xu, Z. Mei, J. Liang, J. Hu, S. Yuan, S. Xiao, Y. Duan, F. Liu, H. Lin, Y. Lin and F. Pan, *ACS Appl. Mater. Interfaces*, 2017, **9**, 29021–29029.
11 D. O. Scanlon, C. W. Dunnill, J. Buckeridge, S. A. Shevlin, A. J. Logsdail, S. M. Woodley, C. R. A. Catlow, M. J. Powell, R. G. Palgrave, I. P. Parkin, G. W. Watson, T. W. Keal, P. Sherwood, A. Walsh and A. A. Sokol, *Nat. Mater.*, 2013, **12**, 798–801.
12 H. X. Zhang, M. Zhao and Q. Jiang, *Appl. Phys. Lett.*, 2013, **103**, 023111.
13 D. Lee and Y. Kanai, *J. Am. Chem. Soc.*, 2012, **134**, 20266–20269.
14 D. Tsukamoto, Y. Shiraishi, Y. Sugano, S. Ichikawa, S. Tanaka and T. Hirai, *J. Am. Chem. Soc.*, 2012, **134**, 6309–6315.
15 U. Diebold, *Surf. Sci. Rep.*, 2003, **48**, 53–229.
16 T. Xia, N. Li, Y. Zhang, M. B. Kruger, J. Murowchick, A. Selloni and X. Chen, *ACS Appl. Mater. Interfaces*, 2013, **5**, 9883–9890.
17 X. Han and G. Shao, *J. Phys. Chem. C*, 2011, **115**, 8274–8282.
18 S. Bakardjieva, N. Murafa, V. Houšková, V. Tyrpekl and V. Štengl, *Appl. Catal., B*, 2009, **89**, 613–619.
19 P. E. Lippens, A. V. Chadwick, A. Weibel, R. Bouchet and P. Knauth, *J. Phys. Chem. C*, 2008, **112**, 43–47.
20 R. Schiller, C. K. Weiss and K. Landfester, *Nanotechnology*, 2010, **21**, 405603.
21 E. Uyanga, A. Gibaud, P. Daniel, D. Sangaa, G. Sevjidsuren, P. Altantsog, T. Beuvier, C. H. Lee and A. M. Balagurov, *Mater. Res. Bull.*, 2014, **60**, 222–231.
22 M. Senthilnanthan, D. P. Ho, S. Vigneswaran, H. H. Ngo and H. K. Shon, *Sep. Purif. Technol.*, 2010, **75**, 415–419.
23 R. G. Nair, A. Das, S. Paul, B. Rajbongshi and S. K. Samdarshi, *J. Alloys Compd.*, 2017, **695**, 3511–3516.
24 H. Mansour, R. Bargougui, A. Gadri and S. Ammar, *J. Mater. Sci.: Mater. Electron.*, 2017, **28**, 1852–1858.
25 C. Y. W. Lin, A. Nakaruk and C. C. Sorrell, *Prog. Org. Coat.*, 2012, **74**, 645–647.
26 H. Y. Hao, C. X. He, B. Z. Tian and J. L. Zhang, *Res. Chem. Intermed.*, 2009, **35**, 705–715.
27 X. Chen and C. Burda, *J. Am. Chem. Soc.*, 2008, **130**, 5018–5019.
28 R. P. Cavalcante, R. F. Dantas, B. Bayarri, O. González, J. Giménez, S. Esplugas and A. Machulek, *Catal. Today*, 2015, **252**, 27–34.
29 D. V. Aware and S. S. Jadhav, *Appl. Nanosci.*, 2016, **6**, 965–972.
30 Y. Lv, L. Yu, H. Huang, H. Liu and Y. Feng, *J. Alloys Compd.*, 2009, **488**, 314–319.
31 K. M. Reddy, B. Baruwati, M. Jayalakshmi, M. M. Rao and S. V. Manorama, *J. Solid State Chem.*, 2005, **178**, 3352–3358.
32 R. Asahi, T. Morikawa, T. Ohwaki, K. Aoki and Y. Taga, *Science*, 2001, **293**, 269–271.
33 D. N. Bui, S. Z. Kang, X. Li and J. Mu, *Catal. Commun.*, 2011, **13**, 14–17.
34 A. A. Murashkina, P. D. Murzin, A. V. Rudakova, V. K. Ryabchuk, A. V. Emeline and D. W. Bahnemann, *J. Phys. Chem. C*, 2015, **119**, 24695–24703.
35 W. Zhao, W. Wang, X. Feng, L. He, Q. Cao, C. Luan and J. Ma, *Ceram. Int.*, 2017, **43**, 8391–8395.
36 K. Sato, Y. Yamauchi, X. Jiang, H. Oveisi, A. Beitollahi, Y. Nemoto and N. Fukata, *J. Nanosci. Nanotechnol.*, 2011, **11**, 6926–6933.
37 S. Chatterjee and A. Chatterjee, *Jpn. J. Appl. Phys.*, 2008, **47**, 1136–1139.
38 F. Sayilkan, M. Asiltürk, P. Tatar, N. Kiraz, Ş. Şener, E. Arpaç and H. Sayilkan, *Mater. Res. Bull.*, 2008, **43**, 127–134.
39 M. Asiltürk, N. Kiraz, F. Sayılkan, E. Arpaç, H. Sayılkan and P. Tatar, *J. Hazard. Mater.*, 2006, **140**, 69–74.
40 V. C. Papadimitriou, V. G. Stefanopoulos, M. N. Romanias, P. Papagiannakopoulos, K. Sambani, V. Tudose and G. Kiriakidis, *Thin Solid Films*, 2011, **520**, 1195–1201.
41 T. M. Grygar, J. Henych, S. Bakardjieva, V. Štengl and J. Velická, *J. Nanomater.*, 2012, 1–11.
42 M. A. Behnajady, B. Alizade and N. Modirshahla, *Photochem. Photobiol.*, 2011, **87**, 1308–1314.
43 Y. Castro and A. Durán, *J. Sol-Gel Sci. Technol.*, 2016, **78**, 482–491.
44 P. Wongwanwattana, P. Krongkitsiri, P. Limsuwan and U. Tipparach, *Ceram. Int.*, 2012, **38**, S517–S519.
45 H. A. Hamedani, N. K. Allam, M. A. El-Sayed, M. A. Khaleel, H. Garmestani and F. M. Alamgir, *Adv. Funct. Mater.*, 2014, **24**, 6783–6796.
46 S. Bouattour, W. Kallel, A. M. Botelho Do Rego, L. F. Vieira Ferreira, I. Ferreira Machado and S. Boufi, *Appl. Organomet. Chem.*, 2010, **24**, 692–699.
47 G. Yang, Z. Yan, T. Xiao and B. Yang, *J. Alloys Compd.*, 2013, **580**, 15–22.
48 Y. Bessekhouad, D. Robert, J. V. Weber and N. Chaoui, *J. Photochem. Photobiol., A*, 2004, **167**, 49–57.
49 T. N. Ravishankar, G. Nagaraju and J. Dupont, *Mater. Res. Bull.*, 2016, **78**, 103–111.
50 L. Elsellami, H. Lachheb and A. Houas, *Mater. Sci. Semicond. Process.*, 2015, **36**, 103–114.
51 Z. Mesgari, M. Gharagozlou, A. Khosravi and K. Gharanjig, *Spectrochim. Acta, Part A*, 2012, **92**, 148–153.
52 Z. Li, W. Shen, W. He and X. Zu, *J. Hazard. Mater.*, 2008, **155**, 590–594.
53 C. He, Y. Yu, X. Hu and A. Larbot, *Appl. Surf. Sci.*, 2002, **200**, 239–247.
54 Y. Li, M. Ma, W. Chen, L. Li and M. Zen, *Mater. Chem. Phys.*, 2011, **129**, 501–505.
55 E. Grabowskaa, M. Diak, T. Klimczuk, W. Lisowski and A. Zaleska-Medynska, *Mol. Catal.*, 2017, **434**, 154–166.

56 J. Q. Bai, W. Wen and J. M. Wu, *CrystEngComm*, 2016, **18**, 1847–1853.
57 J. Kuncewicz and B. Ohtani, *RSC Adv.*, 2016, **6**, 77201–77211.
58 R. López, R. Gómez and M. E. Llanos, *Catal. Today*, 2010, **148**, 103–108.
59 G. Colón, M. Maicu, M. C. Hidalgo and J. A. Navío, *Appl. Catal., B*, 2006, **67**, 41–51.
60 C. Te Hsieh, W. S. Fan, W. Y. Chen and J. Y. Lin, *Sep. Purif. Technol.*, 2009, **67**, 312–318.
61 M. Hamadanian, A. Sadeghi Sarabi, A. Mohammadi Mehra and V. Jabbari, *Mater. Sci. Semicond. Process.*, 2014, **21**, 161–166.
62 I. Cimieri, H. Poelman, J. Ryckaert and D. Poelman, *J. Photochem. Photobiol., A*, 2013, **263**, 1–7.
63 B. Tian, C. Li and J. Zhang, *Chem. Eng. J.*, 2012, **191**, 402–409.
64 X. Ma, L. Xue, S. Yin, M. Yang and Y. Yan, *J. Wuhan Univ. Technol., Mater. Sci. Ed.*, 2014, **29**, 863–868.
65 Y. Cai, X. Chen, Y. Wang, M. Qiu and Y. Fan, *Microporous Mesoporous Mater.*, 2015, **201**, 202–209.
66 A. N. Banerjee, N. Hamnabard and S. W. Joo, *Ceram. Int.*, 2016, **42**, 12010–12026.
67 J. C. S. Wu and C. H. Chen, *J. Photochem. Photobiol., A*, 2004, **163**, 509–515.
68 Alamgir, W. Khan, S. Ahmad, M. Mehedi Hassan and A. H. Naqvi, *Opt. Mater.*, 2014, **38**, 278–285.
69 S. D. Delekar, H. M. Yadav, S. N. Achary, S. S. Meena and S. H. Pawar, *Appl. Surf. Sci.*, 2012, **263**, 536–545.
70 D. V. Wellia, Q. C. Xu, M. A. Sk, K. H. Lim, T. M. Lim and T. T. Y. Tan, *Appl. Catal., A*, 2011, **401**, 98–105.
71 N. H. Nguyen, H. Y. Wu and H. Bai, *Chem. Eng. J.*, 2015, **269**, 60–66.
72 W. F. Chen, H. Chen, P. Koshy, A. Nakaruk and C. C. Sorrell, *Mater. Chem. Phys.*, 2018, **205**, 334–346.
73 P. Benjwal and K. K. Kar, *Mater. Chem. Phys.*, 2015, **160**, 279–288.
74 B. Zhao, J. Wang, H. Li, H. Wang, X. Jia and P. Su, *Phys. Chem. Chem. Phys.*, 2015, **17**, 14836–14842.
75 J.-G. Ma, C.-R. Zhang, J.-J. Gong, Y.-Z. Wu, S.-Z. Kou, H. Yang, Y.-H. Chen, Z.-J. Liu and H.-S. Chen, *Materials*, 2015, **8**, 5508–5525.
76 C. Li, Y. F. Zhao, Y. Y. Gong, T. Wang and C. Q. Sun, *Phys. Chem. Chem. Phys.*, 2014, **16**, 21446–21451.
77 Q. Hou, C. Zhao and L. Qu, *Int. J. Mod. Phys. B*, 2016, **31**, 1650240.
78 H. Peng, J. Li, S. S. Li and J. B. Xia, *J. Phys.: Condens. Matter*, 2008, **20**, 125207.
79 J. W. Pan, C. Li, Y. F. Zhao, R. X. Liu, Y. Y. Gong, L. Y. Niu, X. J. Liu and B. Q. Chi, *Chem. Phys. Lett.*, 2015, **628**, 43–48.
80 K. Yang, Y. Dai and B. Huang, *J. Phys. Chem. C*, 2010, **114**, 19830–19834.
81 M. Harb, P. Sautet and P. Raybaud, *J. Phys. Chem. C*, 2013, **117**, 8892–8902.
82 Y. X. Han, C. L. Yang, M. S. Wang, X. G. Ma and L. Z. Wang, *Sol. Energy Mater. Sol. Cells*, 2015, **132**, 94–100.
83 T. Umebayashi, T. Yamaki, H. Itoh and K. Asai, *Appl. Phys. Lett.*, 2002, **81**, 454–456.
84 C. Di Valentin and G. Pacchioni, *Catal. Today*, 2013, **206**, 12–18.
85 X. D. Liu, E. Y. Jiang, Z. Q. Li and Q. G. Song, *Appl. Phys. Lett.*, 2008, **92**, 2006–2009.
86 R. Long, Y. Dai, G. Meng and B. Huang, *Phys. Chem. Chem. Phys.*, 2009, **11**, 8165–8172.
87 R. Shirley, M. Kraft and O. R. Inderwildi, *Phys. Rev. B: Condens. Matter Mater. Phys.*, 2010, **81**, 075111.
88 W. Kohn and L. J. Sham, *Phys. Rev.*, 1965, **140**, A1133–A1138.
89 G. Kresse and J. Furthmüller, *Comput. Mater. Sci.*, 1996, **6**, 15–50.
90 G. Kresse and J. Furthmüller, *Phys. Rev. B: Condens. Matter Mater. Phys.*, 1996, **54**, 11169–11186.
91 J. P. Perdew, K. Burke and M. Ernzerhof, *Phys. Rev. Lett.*, 1996, **77**, 3865–3868.
92 J. P. Perdew, J. A. Chevary, S. H. Vosko, K. A. Jackson, M. R. Pederson, D. J. Singh and C. Fiolhais, *Phys. Rev. B: Condens. Matter Mater. Phys.*, 1992, **46**, 6671–6687.
93 A. I. Liechtenstein, V. I. Anisimov and J. Zaanen, *Phys. Rev. B: Condens. Matter Mater. Phys.*, 1995, **52**, R5467–R5470.
94 J. Heyd and G. E. Scuseria, *J. Chem. Phys.*, 2004, **121**, 1187–1192.
95 J. Heyd, G. E. Scuseria and M. Ernzerhof, *J. Chem. Phys.*, 2003, **118**, 8207–8215.
96 J. Heyd, G. E. Scuseria and M. Ernzerhof, *J. Chem. Phys.*, 2006, **124**, 219906.
97 M. C. Tsai, J. Rick, W. N. Su and B. J. Hwang, *Mol. Syst. Des. Eng.*, 2017, **2**, 449–456.
98 M. Matsubara, R. Saniz, B. Partoens and D. Lamoen, *Phys. Chem. Chem. Phys.*, 2017, **19**, 1945–1952.
99 M. Harb, P. Sautet and P. Raybaud, *J. Phys. Chem. C*, 2011, **115**, 19394–19404.
100 J. Huang, S. Wen, J. Liu and G. He, *J. Nat. Gas Chem.*, 2012, **21**, 302–307.
101 J. P. Perdew and M. Levy, *Phys. Rev. Lett.*, 1983, **51**, 1884–1887.
102 W. Jia, Z. Cao, L. Wang, J. Fu, X. Chi, W. Gao and L. W. Wang, *Comput. Phys. Commun.*, 2013, **184**, 9–18.
103 W. Jia, J. Fu, Z. Cao, L. Wang, X. Chi, W. Gao and L. W. Wang, *J. Comput. Phys.*, 2013, **251**, 102–115.
104 M. Schlipf and F. Gygi, *Comput. Phys. Commun.*, 2015, **196**, 36–44.
105 D. R. Hamann, *Phys. Rev. B: Condens. Matter Mater. Phys.*, 2013, **88**, 085117.
106 H. J. Monkhorst and J. D. Pack, *Phys. Rev. B: Condens. Matter Mater. Phys.*, 1976, **13**, 5188–5192.
107 M. Horn, C. F. Schwerdtfeger and E. P. Meagher, *Z. Kristallogr. - New Cryst. Struct.*, 1972, **136**, 273–281.
108 D. T. Cromer and K. Herrington, *J. Am. Chem. Soc.*, 1955, **77**, 4708–4709.
109 D. Dash, S. Chaudhury and S. K. Tripathy, in *Advances in Communication, Devices and Networking*, ed. R. Bera, S. K. Sarkar and S. Chakraborty, Springer, Singapore, Singapore, 2018, pp. 57–67.

110 C. Qiang and C. Hong-Hong, *Chin. Phys.*, 2004, **13**, 2121–2125.
111 Z. Wang, U. Helmersson and P.-O. Käll, *Thin Solid Films*, 2002, **405**, 50–54.
112 S. Vyas, R. Tiwary, K. Shubham and P. Chakrabarti, *Superlattices Microstruct.*, 2015, **80**, 215–221.
113 M. Khan, J. Xu, W. Cao and Z.-K. Liu, *J. Nanosci. Nanotechnol.*, 2014, **14**, 6865–6871.
114 E. B. Gracien, J. Shen, X. R. Sun, D. Liu, M. Li, S. D. Yao and J. Sun, *Thin Solid Films*, 2007, **515**, 5287–5297.
115 M. M. Mahlambi, A. K. Mishra, S. B. Mishra, R. W. Krause, B. B. Mamba and A. M. Raichur, *Ind. Eng. Chem. Res.*, 2013, **52**, 1783–1794.
116 K. Yang, Y. Dai and B. Huangl, *ChemPhysChem*, 2009, **10**, 2327–2333.